A nutrient increment method for reducing bias in global biogeochemical models

J. While,[1,2] K. Haines,[1] and G. Smith[1,3]

Received 22 January 2010; revised 21 June 2010; accepted 30 June 2010; published 16 October 2010.

[1] Assimilation of physical variables into coupled physical/biogeochemical models poses considerable difficulties. One problem is that data assimilation can break relationships between physical and biological variables. As a consequence, biological tracers, especially nutrients, are incorrectly displaced in the vertical, resulting in unrealistic biogeochemical fields. To prevent this, we present the idea of applying an increment to the nutrient field within a data assimilating model to ensure that nutrient-potential density relationships are maintained within a water column during assimilation. After correcting the nutrients, it is assumed that other biological variables rapidly adjust to the corrected nutrient fields. We applied this method to a 17 year run of the 2° NEMO ocean-ice model coupled to the PlankTOM5 ecosystem model. Results were compared with a control with no assimilation, and with a model with physical assimilation but no nutrient increment. In the nutrient incrementing experiment, phosphate distributions were improved both at high latitudes and at the equator. At midlatitudes, assimilation generated unrealistic advective upwelling of nutrients within the boundary currents, which spread into the subtropical gyres resulting in more biased nutrient fields. This result was largely unaffected by the nutrient increment and is probably due to boundary currents being poorly resolved in a 2° model. Changes to nutrient distributions fed through into other biological parameters altering primary production, air-sea CO_2 flux, and chlorophyll distributions. These secondary changes were most pronounced in the subtropical gyres and at the equator, which are more nutrient limited than high latitudes.

Citation: While, J., K. Haines, and G. Smith (2010), A nutrient increment method for reducing bias in global biogeochemical models, *J. Geophys. Res.*, *115*, C10036, doi:10.1029/2010JC006142.

1. Introduction

[2] The motivation for the study presented here is to improve the behavior of biogeochemical models of the ocean by running them embedded within models of ocean physics enhanced with data assimilation. Physical properties, such as temperature and mixed layer depth, of ocean models are now routinely improved through the use of data assimilation at operational forecast centers such as the UK Met Office [see, e.g., *Martin et al.*, 2007]. However, data assimilation in physical ocean models with embedded biogeochemistry presents additional challenges, some of which we address in this paper.

[3] There has been surprisingly little work published that has focused on the use of data assimilation in correcting the physical ocean state in biogeochemical modeling. However, *Eden and Oschlies* [2006] used the semiprognostic method of data assimilation to constrain the circulation of the North Atlantic, which resulted in improved estimates of CO_2 flux, particularly through improvements in the Gulf Stream path. Physical and biological assimilation are applied to a mesoscale feature by *Anderson et al.* [2000], who show that the best results are obtained when physical and biological assimilation are applied together. If one form of assimilation is applied without the other, a misalignment of physical and biological fronts can occur. It is a similar problem, whereby assimilation of physical processes upsets nutrient balances in the biological system, which is the focus of this paper.

[4] More work has focused on assimilating biological variables alone. This is done for both parameter [e.g., *Losa et al.*, 2003; *Zhao et al.*, 2005; *Ridgwell et al.*, 2007] and state estimation. In most cases, due to a lack of other readily available data, satellite-derived chlorophyll is used as the data source for assimilation. That such methods can be effective is demonstrated using twin experiments by *Carmillet et al.* [2001] and, for the North Atlantic, using real data of *Natvik and Evensen* [2002]. The assimilation of real global chlorophyll data is reported by both *Nerger and Gregg* [2007] and *Gregg* [2007]; in both cases, reduced error with respect to in situ measurements was demonstrated. A problem with chlorophyll assimilation is that

[1]Environmental Systems Science Centre, University of Reading, Reading, UK.
[2]Now at UK Met Office, Exeter, UK.
[3]Now at Management Research Division/Atmospheric Science and Technology Directorate, Environment Canada, Dorval, Quebec, Canada.

0148-0227/10/2010JC006142

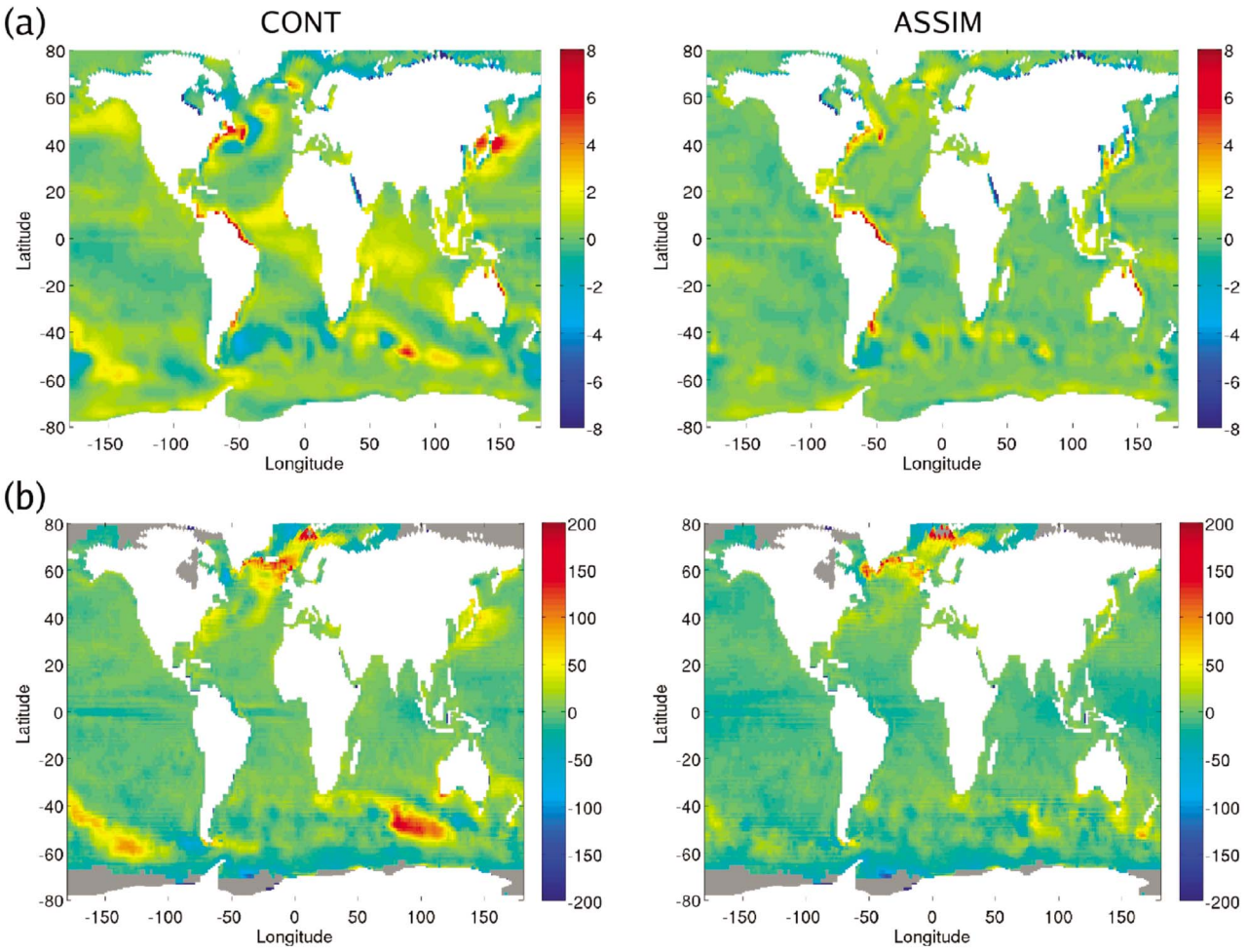

Figure 1. Mean, averaged over the analysis period and down to 313 m depth (18 model levels), bias in model temperature and MLD. (a) The difference between model temperature and the WOA05 climatology [*Locarnini et al.*, 2006]. (b) Comparison of the model MLD with the climatology of *de Boyer Montégut et al.* [2004]. Results shown are from (left) CONT and (right) ASSIM. Units are °C for temperature and m for MLD.

chlorophyll data are only a proxy for the distribution of phytoplankton, and they do not give direct information about the state of the rest of the biological system. In particular, nutrients, which are critical to productivity, are not constrained by chlorophyll data. To get around this, *Hemmings et al.* [2008] describe a nitrogen balancing method, applied during assimilation, that attempts to maintain a realistic nitrogen distribution between the components of a nutrient phytoplankton zooplankton detritus (NPZD) model.

[5] Ocean nutrients are a key determining factor in the distribution of ocean life [*Beardall et al.*, 2001], and in this paper we focus on the effects that physical data assimilation has on model nutrient fields. Although physical data assimilation is demonstrably able to improve the physical ocean state [see, e.g., *Smith and Haines*, 2009; *Martin et al.*, 2007; *Ming and Leetmaa*, 1997; *Fox and Haines*, 2003], it is less clear that nutrient or phytoplankton (chlorophyll) fields can be similarly improved. Nonetheless, it is expected that physical data assimilation methods could be modified such that they produce improved ocean nutrient fields. In principle, conventional multivariate data assimilation can be applied directly to nutrients, along with assimilation of ocean temperature and salinity (as is done by *Anderson et al.* [2000]). However, there are few nutrient measurements available from which we can derive the necessary multivariate correlations. An alternative approach is suggested by *Troccoli and Haines* [1999]. In this paper, temperature profile measurements are assimilated and then salinity is adjusted such that a salinity-temperature relationship is maintained in each water column. *Haines et al.* [2006] presented results demonstrating that a large part of measured salinity variability can be captured by such a method, without any resort to direct assimilation of salinity data. In this paper we apply similar ideas to ocean nutrients, in that a "nutrient increment" is applied to an ocean model such that nutrient-potential density relationships are maintained. Specifically, we present results from an experiment constructed to test the hypothesis that a nutrient increment in a model assimilating physical data can improve nutrient distributions and the associated biogeochemistry. The experiment consisted of three runs: a control, a standard assimilating

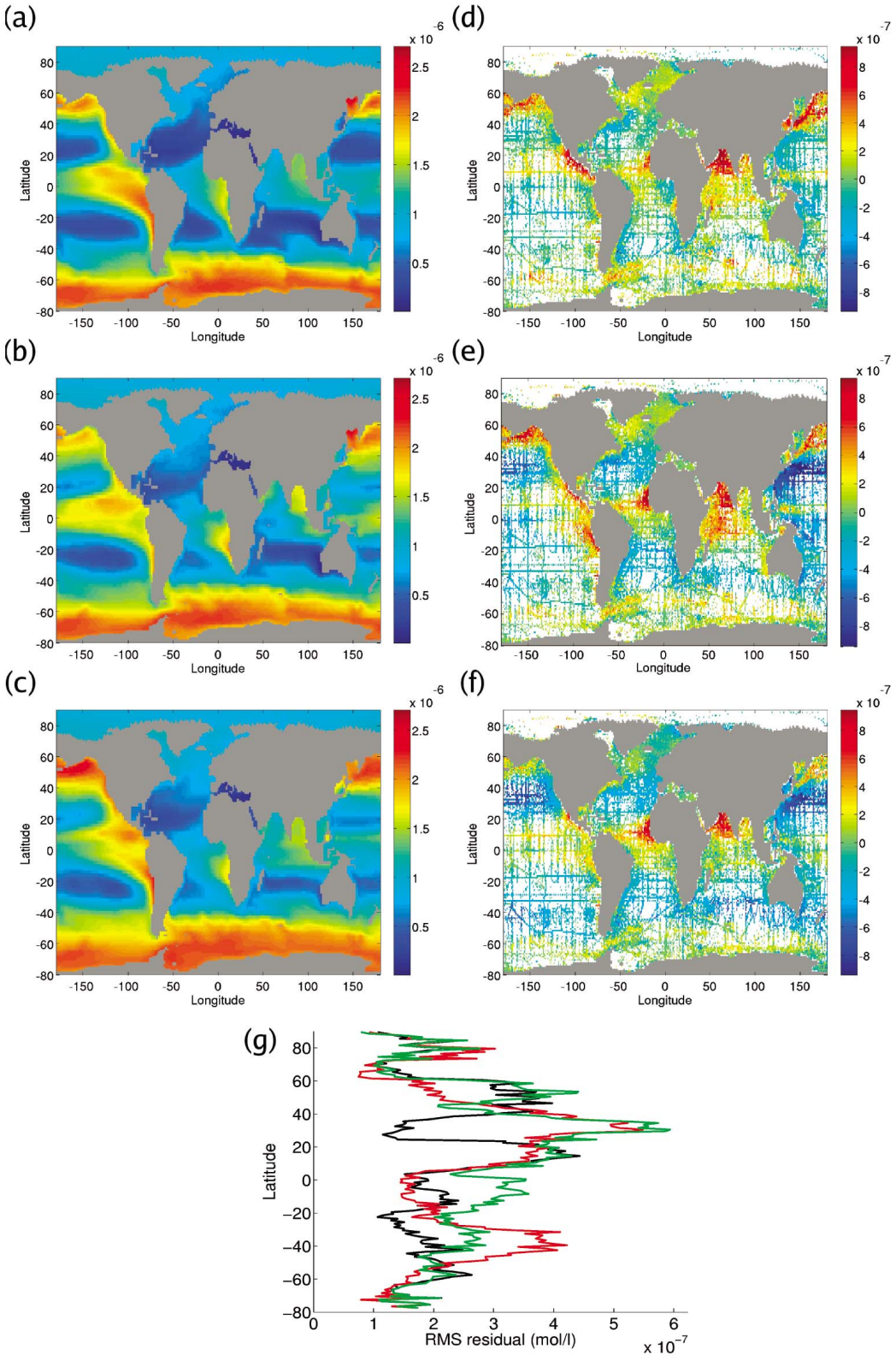

Figure 2. Model phosphate (in mol/L) averaged down to 313 m depth (18 model levels) and over the analysis period. Shown at left are model phosphate for (a) CONT, (b) ASSIM, and (c) NINC. Shown at right are World Ocean Database [*Garcia et al.*, 2006] mean phosphate minus (d) CONT, (e) ASSIM, and (f) NINC. (g) The latitudinal RMS difference between WOD05 and (black) CONT, (red) NINC, and (green) ASSIM.

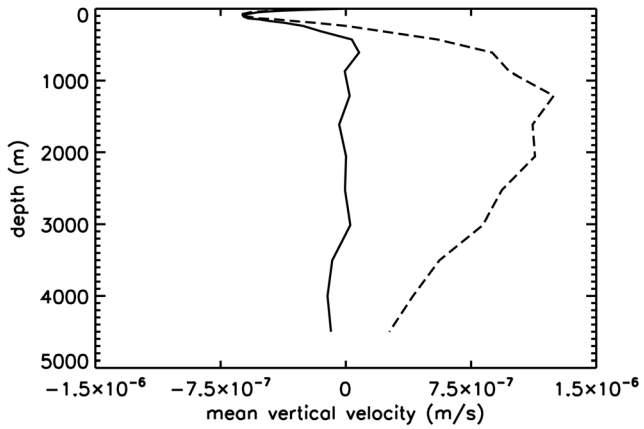

Figure 3. Mean upward vertical velocity against depth of CONT (solid curve) and ASSIM (dashed curve) around the Kuroshio. Velocities were averaged over the region 120°E–160°E, 20°N–50°N, and over the entire run period of our experiments.

run, and a run that included a nutrient increment alongside the physical data assimilation. The results of this experiment, presented in detail below, showed that the nutrient increment significantly reduced nutrient bias in both equatorial waters and at high latitudes, although large biases still remained in the subtropical gyres. Changes to the nutrient field impacted upon the biological state of the ocean; thus results detailing changes to the modeled ocean biogeochemistry are also presented.

[6] The paper is laid out as follows. Section 2 discusses the models used (NEMO and PlankTOM5), outlines the optimal interpolation data assimilation method, describes the nutrient increment technique, and details the experiments performed. Results are presented in section 3, and the paper concludes with a discussion in section 4.

2. Experimental Framework

2.1. Physical Model: NEMO 2°

[7] In all experiments described here we have used version 2.3 of the NEMO (Nucleus for European Modeling of the Ocean) modeling framework. This framework includes the OPA9 [*Madec*, 2008] ocean general circulation model and the LIM2 ice model (described by *Fichefet and Morales Maqueda* [1997, 1999]). OPA9 is a primitive equation model that solves, in a Boussinesq approximation, the hydrostatic Navier-Stokes equations. All experiments were conducted using the global ORCA 2° version of the NEMO grid. The unique characteristic of ORCA is that it is a tripolar curvilinear grid and avoids the singularity at the North Pole, while giving increased resolution over the Arctic. This model configuration has a resolution of approximately 2° in both latitude and longitude, with higher resolution near the equator and in select regions, such as the Mediterranean. In the vertical there are 31 levels, with 10 m resolution in the near surface. Full layer thickness cells are used at the ocean bottom, as difficulties with the biology were encountered when using the more realistic partial cells. The momentum and continuity equations are solved using a forward time differencing scheme for the horizontal diffusion, an implicit scheme for the vertical diffusion, and a leap-frog scheme for the other terms. The active tracer advection is computed using a total variance diminishing scheme (described by *Zalesak* [1979]), while advection of passive tracers, such as biological variables, is integrated forward using a Smolarkiewicz scheme [*Smolarkiewicz*, 1983]. Concurrently, diffusion is calculated with a forward scheme horizontally and an implicit scheme vertically. In addition to this, the model uses the *Gent and McWilliams* [1990] advective eddy parameterization.

[8] Forcing fields applied to the model were taken from the DFS3 (DRAKKAR Forcing Set 3) data set. This is a hybrid data set based on ERA40 [*Uppala et al.*, 2005] and CORE [*Large and Yeager*, 2004] that runs between 1958 and 2004; it is described in full by *Brodeau et al.* [2009]. To extend this forcing out to 2007, we have used the ECMWF (European Centre for Medium Range Weather Forecasts) operational analysis for winds and air temperatures.

2.2. Biogeochemical Model: PlankTOM5

[9] Biogeochemistry in our model runs is based on the PlankTOM5 model. This is part of the DGOM (dynamic green ocean model) suit of models that are described by *Le Quéré et al.* [2005]. PlankTOM5 itself is an iron limited plankton functional type model and includes five plankton types: coccolithophores (calcifiers), diatoms (silicifiers), a mixed phytoplankton type, mesozooplankton (200–2000 μm in size), and microzooplankton (size <200 μm). PlankTOM5 also models the nutrients silicate, phosphate, and iron, where phosphate and iron are limiting to all phytoplankton groups, and silicate is only limiting to diatoms. Nitrogen within the model is linked to the phosphate distribution with a fixed nitrate/phosphate ratio of 16:1. PlankTOM5 also includes a representation of the carbon cycle and alkalinity, with dissolved inorganic carbon (DIC), dissolved organic carbon (DOC), and two size classes of particulate organic carbon modeled. The air-sea carbon flux is calculated using the parameterizations of *Sweeny et al.* [2007]; this is a modification to the baseline PlankTOM5 code which uses the *Wanninkhof* [1992] parameterization. All of these processes within PlankTOM5 are described by their own set of equations and parameters. A description of these equations for an early version of the model (PISCES) is given by *Aumont et al.* [2003] and *Buitenhuis et al.* [2006] or is available online at http://lgmacweb.env.uea.ac.uk/green_ocean.

2.3. Experimental Details

[10] In this paper we report results from three numerical experiments: a control run CONT, an assimilation run ASSIM, and a nutrient incrementing run NINC. CONT was initialized in 1990 from mean temperature and salinity fields taken from the 2005 version of the World Ocean Atlas (WOA05) [*Locarnini et al.*, 2006; *Antonov et al.*, 2006]. For the biogeochemical part of the model, such nutrients as are available were also initialized from WOA05 climatologies [*Garcia et al.*, 2006]. Other biological fields, for which a climatological state was not available, were initialized from the output of an earlier spin-up run of the PlankTOM5 model conducted at the University of East Anglia (Erik Buitenhuis, personal communication, 2007). CONT was run for 10 years until 2000 to spin up ocean currents. The subsequent 7 years

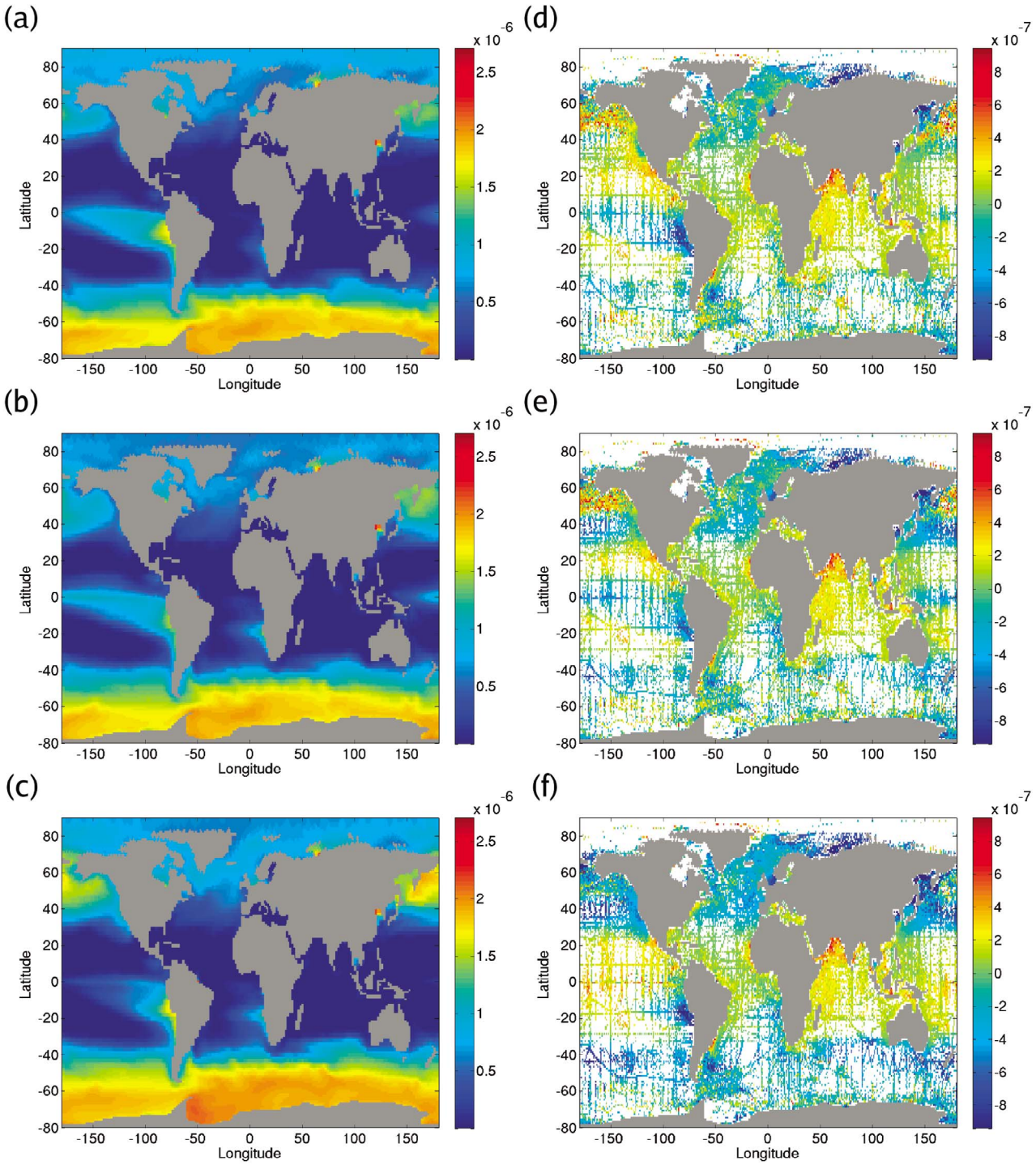

Figure 4. Near-surface model phosphate (in mol/L) averaged down to 20 m depth (two model levels) and over the analysis period. Shown at left are model phosphate for (a) CONT, (b) ASSIM, and (c) NINC. Shown at right are World Ocean Atlas [*Garcia et al.*, 2006] mean phosphate minus (d) CONT, (e) ASSIM, and (f) NINC.

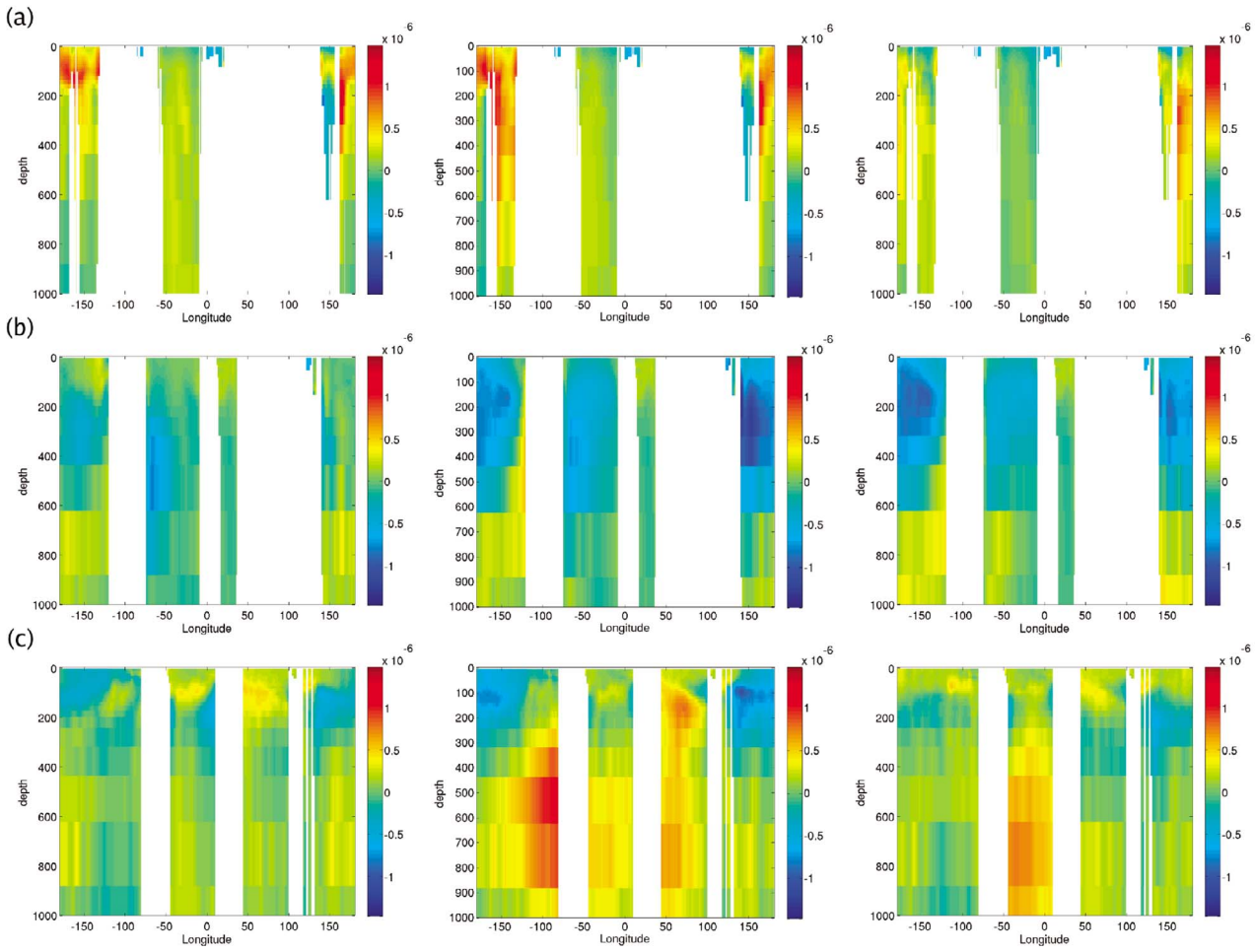

Figure 5. Depth slices of WOA05 phosphate climatology minus model phosphate (in mol/L). Plots are from (a) 55°N, (b) 35°N, and (c) the equator. The results from (left) CONT, (middle) ASSIM, and (right) NINC. All results shown are an average over the entire analysis period.

of the run (2000 until 2007) constituted an analysis period from which our results are taken. Output from CONT consisted of 30 day means of the physical and biological fields.

[11] ASSIM and NINC were identical to CONT except in the assimilation of data. In both ASSIM and NINC, observed hydrographic data were assimilated, but only in NINC were updates applied to the nutrient fields. Specifically, temperature and salinity data were assimilated from the start of both runs using the scheme described in section 2.4. Additionally, phosphate, being the main controlling nutrient of the PlankTOM5 model, was updated in NINC using the nutrient increment method described in section 2.5, while the other nutrients, iron and silicate, were left to evolve freely. In the case of silicate this was partly due to large, poorly resolved, silicate-density gradients at depth, which make it extremely difficult to calculate silicate increments in this way.

2.4. Physical Assimilation Scheme

[12] The observations assimilated in NINC and ASSIM are hydrographic profile data taken from the ENSEMBLES 3 data set [*Ingleby and Huddleston*, 2007]. Assimilation was performed using the methodology of *Haines et al.* [2006] and *Smith and Haines* [2009]. This is an optimal interpolation technique that assimilates both temperature and salinity data. However, instead of assimilating temperature and salinity jointly, a multiple stage approach is applied. First, temperature is assimilated; this is followed by a salinity correction, as described by *Troccoli and Haines* [1999], to maintain salinity-temperature relationships within each water column. Finally, any available salinity observations are assimilated; however, now salinity assimilation takes place along isotherms, as in the work by *Haines et al.* [2006].

[13] This procedure affords us two advantages: First, by evaluating salinity errors on isotherms rather than isobaths, much of the dynamical variability (i.e., heaving of water up and down) of salinity is removed. Second, assimilation increments to salinity can be spread along isotherms, as opposed to isobaths; this naturally confines an assimilation increment to a particular water mass and prevents information spreading to neighboring, but distinct, water masses.

[14] On a practical level, model minus data differences (innovations) were obtained from the model at the closest time step to each observation. Innovations were then accumulated over 5 days before being converted into analysis increments. An incremental analysis update method [*Bloom*

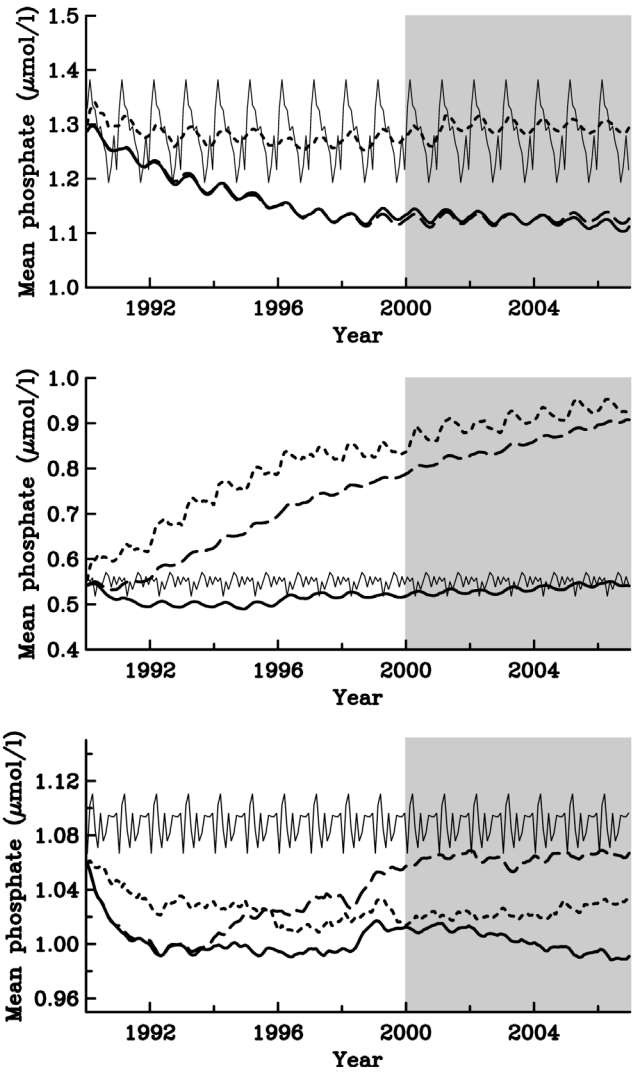

Figure 6. Time series of mean phosphate from 1990 until the end of the experiment for three latitude bands: (top) 45°N–90°N, (middle) 20°N–45°N, and (bottom) 20°S–20°N. These regions reflect results from high latitudes, the gyres, and the equator, respectively. The solid curves are from CONT, the short-dashed curves are from NINC, the long-dashed curves are from ASSIM, while the thin curves are the WOA05 phosphate climatology. In each plot the region highlighted in light gray is the analysis period of the run. All results are an average through the top 313 m (18 model levels) of the ocean.

et al., 1996] was then used to insert the analysis increments into the model over one model day.

2.5. Nutrient Assimilation Scheme

[15] *While and Haines* [2010] demonstrates that over most of the ocean a nutrient-density relationship exists for phosphate, silicate, and nitrate, a relationship that is broken by physical data assimilation. To prevent this, we define a nutrient increment that maintains nutrient density relationships. It is this increment that is applied in experiment NINC. The increment ΔN_I can be defined as

$$\Delta N_I = N^{\mathrm{f}}(\sigma^{\mathrm{a}}) - N^{\mathrm{f}}(\sigma^{\mathrm{f}}), \tag{1}$$

where σ is the potential density (referenced to 2000 m), and $N(\sigma)$ is the nutrient value, within a water column, at density σ. We use superscript a to denote analysis, with f for forecast. In our experiments, linear interpolation is used to estimate $N^{\mathrm{f}}(\sigma^{\mathrm{a}})$, and $N^{\mathrm{f}}(\sigma^{\mathrm{f}})$ is known directly from the model forecast; thus, at a depth level k, where $k = 0, 1, 2, \ldots$ measured from the surface, the nutrient analysis N^{a} is

$$N^{\mathrm{a}}_k = \frac{(\sigma^{\mathrm{a}}_k - \sigma^{\mathrm{f}}_{k0})(N^{\mathrm{f}}_{k1} - N^{\mathrm{f}}_{k0})}{(\sigma^{\mathrm{f}}_{k1} - \sigma^{\mathrm{f}}_{k0})}, \tag{2}$$

where $k0$ and $k1 = k0 + 1$ are the model levels that, in the forecast, bracket the density σ^{a}_k. Difficulties can arise in the surface mixed layer where stratification is very low, so N^{a} is only calculated below 100 m depth.

3. Results

3.1. Temperature and Mixed Layer Depth

[16] The most important physical properties of the model run, in terms of their effect on ocean biology, are the temperature and mixed layer depth (MLD). Consequently, a principle aim of assimilating data must be to improve these properties. In Figure 1 we show the temperature and MLD bias of CONT and ASSIM (results from NINC are identical to those from ASSIM) when compared with the temperature climatology of WOA05 [*Locarnini et al.*, 2006] and the MLD climatology of *de Boyer Montégut et al.* [2004]. For temperature the results are the average of the top 313 m (18 model levels) of the ocean. Note that the MLD provided by the NEMO model has a different depth criterion than the climatology (a density difference of 0.01 kg/m^3 from the surface, as opposed to 0.03 kg/m^3 for *de Boyer Montégut et al.* [2004]), which means that a perfect model and climatology would show a universal small negative bias.

[17] In Figure 1 the temperature bias has been unambiguously reduced almost everywhere in NINC, with the exception of some coastal regions where we do not assimilate data and which are poorly resolved by the ORCA2 model. The bias in MLD is also reduced in most regions, with the biggest improvements seen in the southern oceans. These results are consistent with the results of *Smith and Haines* [2009], where a higher model resolution was used.

3.2. Phosphate

[18] Mean phosphate distributions, averaged down to 313 m and over the 7 year analysis period, of CONT, ASSIM, and NINC are shown in Figure 2. Additionally, by subtracting model phosphate from WOA05 values, biases with respect to the WOA05 mean phosphate [*Garcia et al.*, 2006] are also shown. From these plots it can be seen that over much of the ocean NINC has substantially smaller biases in phosphate than either CONT or ASSIM. Biases are significantly reduced in the North Pacific, North Atlantic, equatorial Pacific (especially with respect to ASSIM), the Indian Ocean, and in the far southern oceans. In some regions, most notably near the west African coast and in the Southern

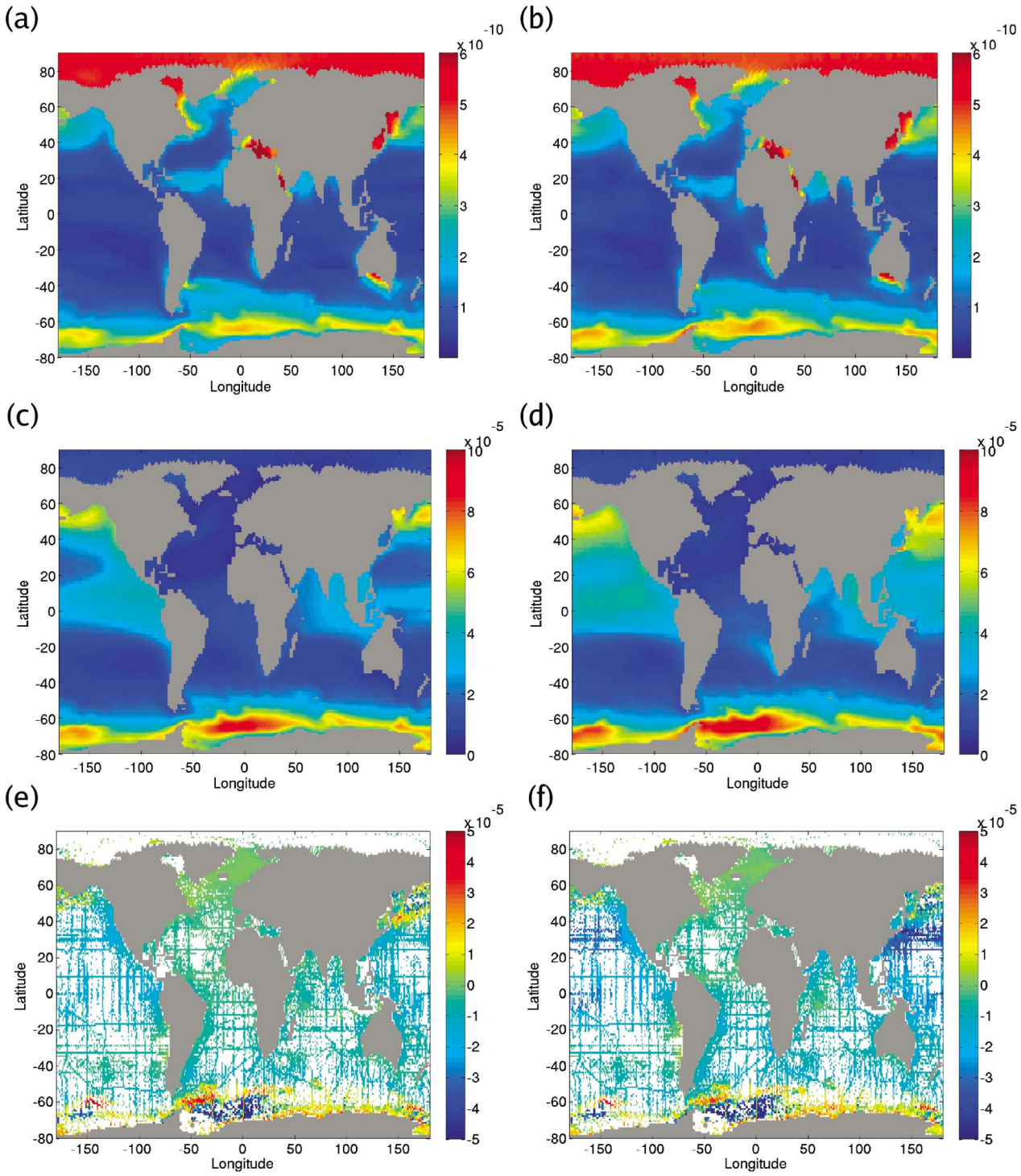

Figure 7. Mean iron and silicate distributions (in mol/L) for our model runs averaged over the analysis period and down to 313 m depth (18 model levels). Top plots show the distribution of iron for (a) CONT and (b) NINC. Middle plots show silicate distributions for (c) CONT and (d) NINC. The bottom plots show WOA05 silicate minus model silicate for (e) CONT and (f) NINC.

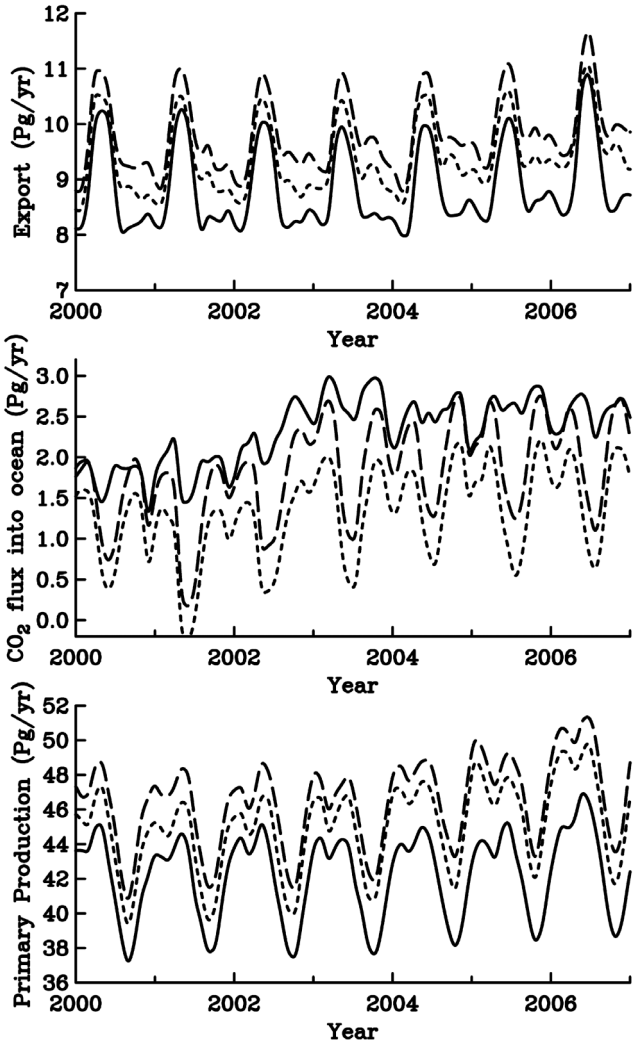

Figure 8. (top) Globally averaged export, (middle) air-to-sea CO_2 flux, and (bottom) primary production of CONT (solid curve), NINC (short-dashed curve), and ASSIM (dashed curve).

Ocean, NINC is not significantly different, or is even slightly worse, than ASSIM, indicating that the nutrient increment is not compensating for nutrient biases in these regions. The poorest results occur in the subtropical gyres, where both NINC and ASSIM have much larger phosphate biases than CONT. A detailed look at the model has found anomalously large vertical velocities in the western boundary currents, especially the Kuroshio, when physical data assimilation is applied. This is demonstrated in Figure 3 where mean vertical velocity for the Kuroshio region (the area enclosed within 120°E–160°E and 20°N–50°N) is shown against depth. Results are shown for CONT and ASSIM, and reveal that below 200 m ASSIM has dramatically higher mean upward vertical velocity than CONT. This velocity acts to advect material to the near surface where it is then diffused around the gyres, causing the phosphate biases. The origin of the excess vertical velocity must be due to perturbations to the model from the assimilation. We speculate that within the boundary currents data assimilation is continuously forcing the model toward a state, in terms of the positioning of fronts and their gradients, that simply cannot be supported in a 2° model. One response of the model to this forcing are the observed excess upward velocities.

[19] Figure 2g shows the zonally averaged RMS difference between our three model runs and WOA05. As expected from the discussion above, both NINC and ASSIM show much larger RMS errors in subtropical gyre latitudes than does CONT. In the Northern Hemisphere subtropical gyres (20°N–40°N), the RMS errors in ASSIM and NINC are much the same, indicating that the nutrient increment is having little impact upon the assimilation induced bias. In the Southern Hemisphere (30°S–55°S), ASSIM has a lower error than NINC and it appears that the nutrient increment directly contributes to the bias. This may be because the assumptions behind the nutrient increment are not valid in the southern gyres; however, nutrient data are very sparse in the Southern Hemisphere and we should treat results from this region with caution. Away from the subtropical gyres, NINC generally outperforms ASSIM in terms of RMS error. This is especially true near the equator where differences are

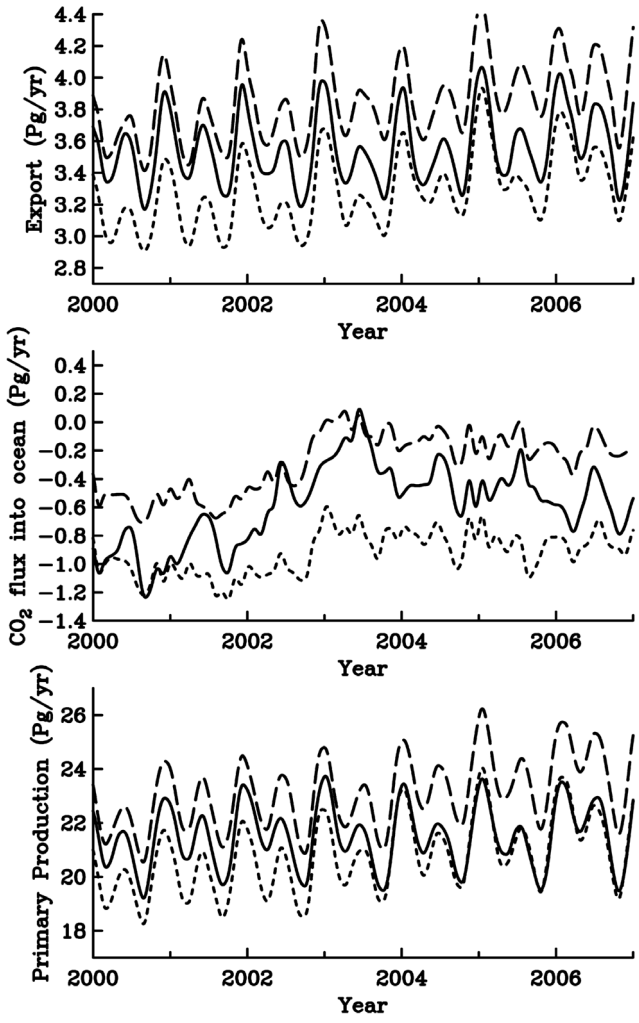

Figure 9. As in Figure 8, but for equatorial waters (20°S–20°N).

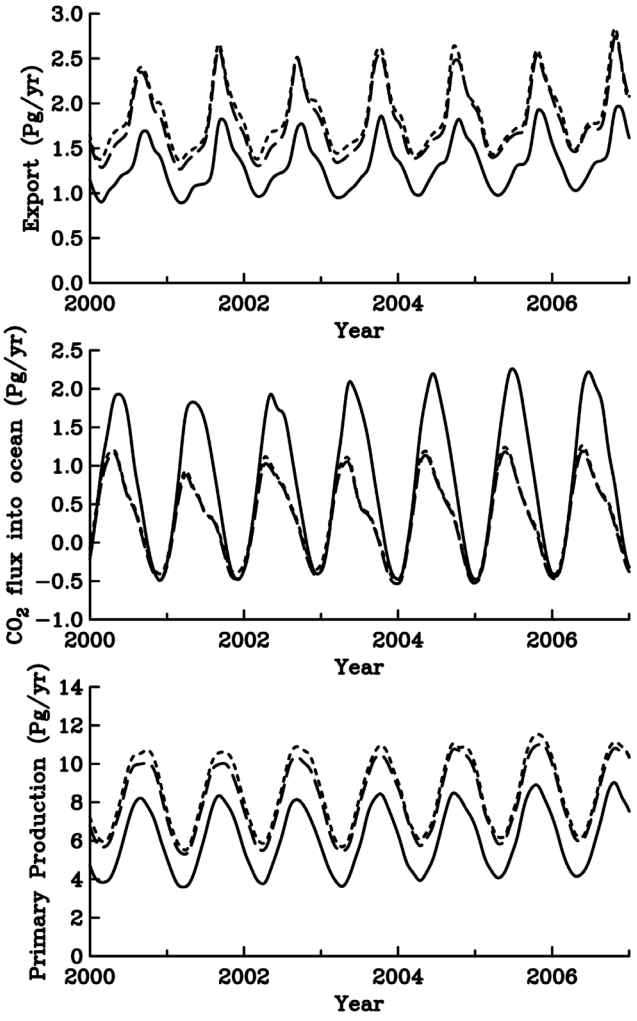

Figure 10. As in Figure 8, but for northern midlatitudes (20°N–45°N).

much smaller than with ASSIM and only apparent south of the equator down to 20°S. Between 40°N and 70°N, CONT has significantly larger errors than NINC and performs almost as poorly as ASSIM. Thus we can conclude that the deficiency with the physical/biogeochemical model at high latitudes is well compensated for by the nutrient increment.

[20] As well as depth-averaged nutrients it is also useful to examine the near-surface nutrient field, which can have a disproportionate impact on ocean biology. Figure 4 is similar to Figure 2 and shows the mean nutrient distribution and its error with respect to WOA05 for the near surface (top 20 m) of the ocean. Ignoring the gyres, Figure 4 shows that the nutrient increment does act to correct the high-latitude and equatorial biases, but that it is slightly overcompensating and producing bias of the opposite sign, particularly in the Southern Hemisphere. Figure 5 shows biases in CONT, ASSIM, and NINC against WOA05 for three different zonal sections through the ocean: 55°N, 35°N, and the equator. Discounting 35°N, which is in the gyres, neither the equatorial or 55°N plot show large biases in NINC that extend to depth. At the equator, ASSIM has huge biases not seen in CONT. These biases change sign with depth and are largely eliminated in NINC, demonstrating that the nutrient increment is indeed preventing the assimilation from unrealistically mixing phosphate. Elsewhere the climatology in the Atlantic has more phosphate than NINC below 400 m, suggesting that the nutrient increment is allowing too little phosphate to upwell from depth. Nonetheless, in the top 200 m of the ocean NINC does appear to show less bias than CONT. At 55°N the underestimate (positive anomaly) of phosphate in CONT, which is driven to even greater depths by assimilation in ASSIM, has been much reduced in NINC, with only the western Pacific still showing some residual error. The 35°N slice is within the subtropical gyres and both ASSIM and NINC significantly overestimate phosphate (negative anomaly) down to 600 m, with positive anomalies below this. However, it should be noted that in the Atlantic NINC does notably better than ASSIM at depths less than 600 m, while being slightly worse at greater depths. More significantly, between 300 m and 900 m in the same region NINC also has smaller anomalies than CONT. Thus we speculate that in the Atlantic, at least some of the error in the subtropical gyres is caused by breaking water mass balances and that the nutrient increment is capable of partially reducing this.

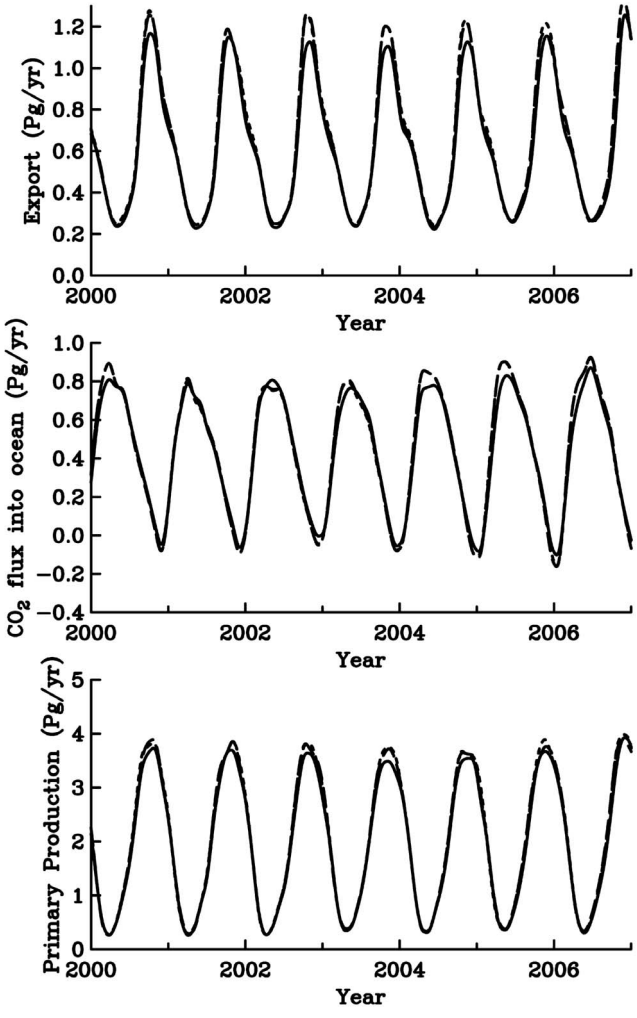

Figure 11. As in Figure 8, but for northern high latitudes (45°N–90°N).

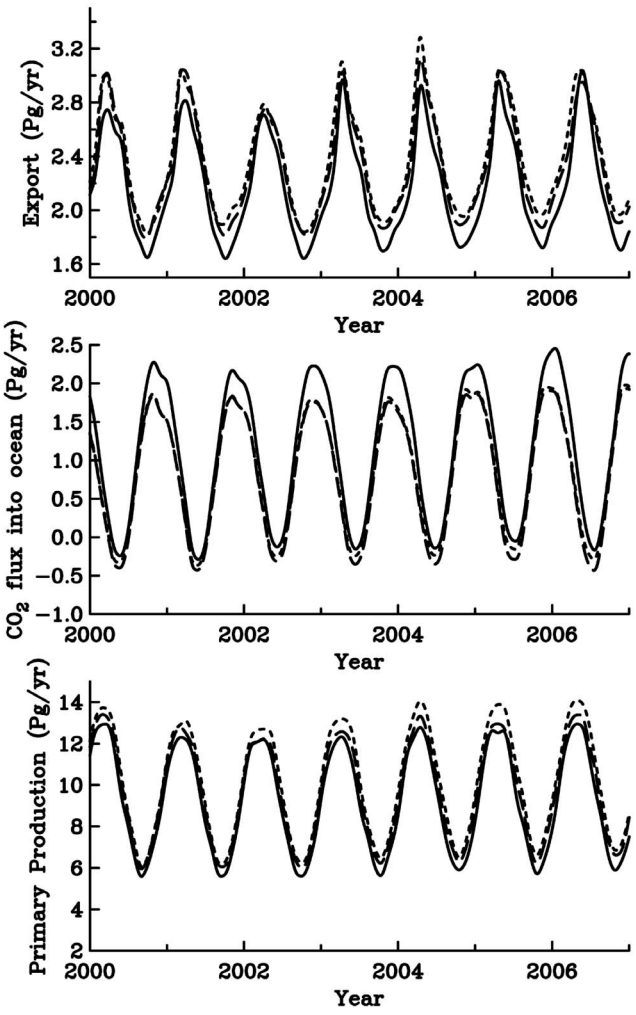

Figure 12. As in Figure 8, but for southern midlatitudes (45°S–20°S).

[21] The temporal evolution of phosphate at the equator, in the subtropical gyres, and at high northern latitudes is shown in Figure 6 for the entire period of our experiments, including the spin-up phase. Results are shown for CONT, ASSIM, NINC, and the climatology of WOA05. The biases already discussed for these regions are clearly seen in Figure 6. At high latitudes both CONT and ASSIM drift away from climatology over a period of 10 years, while there is almost no drift in NINC. This indicates that the nutrient increment is preventing unrealistic nutrient loss. The nutrient increment has a similar effect on NINC phosphate at the equator, but is not sufficient to prevent the model progressively underestimating phosphate relative to climatology. In fact, shortly after 1000 days ASSIM becomes closer to climatology than NINC. An investigation of Figure 2 shows this result to be spurious; in reality NINC is less biased than ASSIM, but in ASSIM a large positive anomaly in the Indian Ocean compensates for negative biases in the Pacific. Finally, within the subtropical gyres CONT underestimates phosphate immediately after initialization, probably as a result of initialization shock, before beginning a slow almost linear trend of increasing phosphate. However, an extreme positive phosphate bias is apparent in both NINC and ASSIM, with phosphate levels rising throughout the run. Toward the end of the analysis period the rate of increase of phosphate in NINC and ASSIM is reducing; this is mainly due to increased surface phosphate distributions driving additional biological export.

[22] On shorter time scales, Figure 6 shows that CONT, ASSIM, and NINC have significantly smaller seasonal cycles than the climatology. This is true both at the equator and at high latitudes. Interestingly, within the subtropical gyres (Figure 6, middle), the climatology, CONT and ASSIM have low seasonal variability, while NINC displays a clear seasonal cycle. Furthermore, the seasonal cycles of NINC and CONT both appear to be out of phase with that of the climatology. One possibility is that in NINC, and to a lesser extent in CONT, increased nutrient availability (including increased silicate; see below) is allowing a seasonal cycle in biogeochemical processing of phosphate. Conversely, in the climatology purely physical processes dominate and these are out of phase with the biogeochemical processes of our model runs. However, we would expect biogeochemical

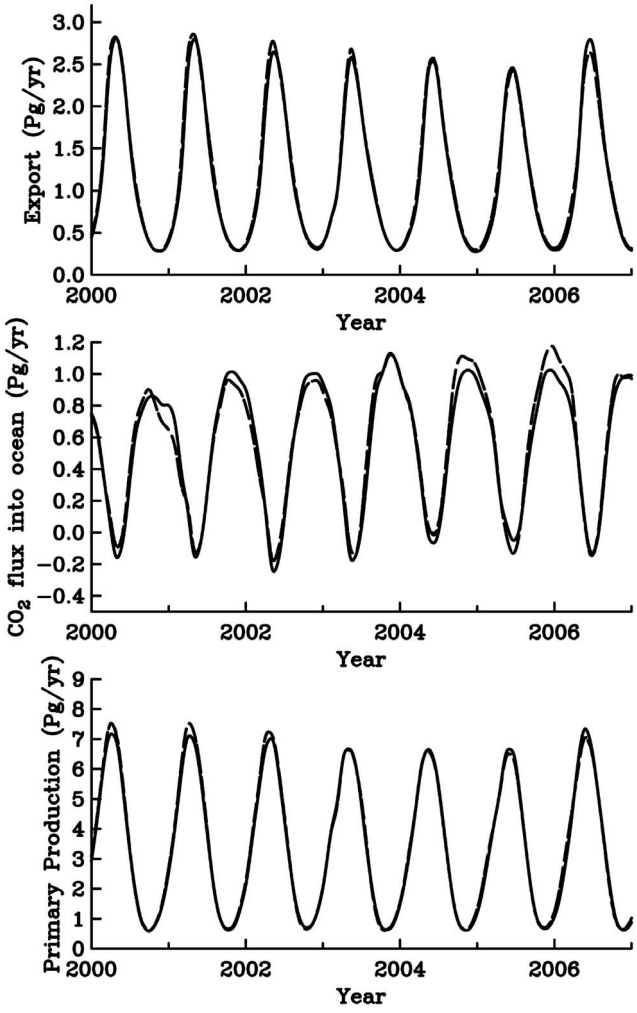

Figure 13. As in Figure 8, but for southern high latitudes (90°S–45°S).

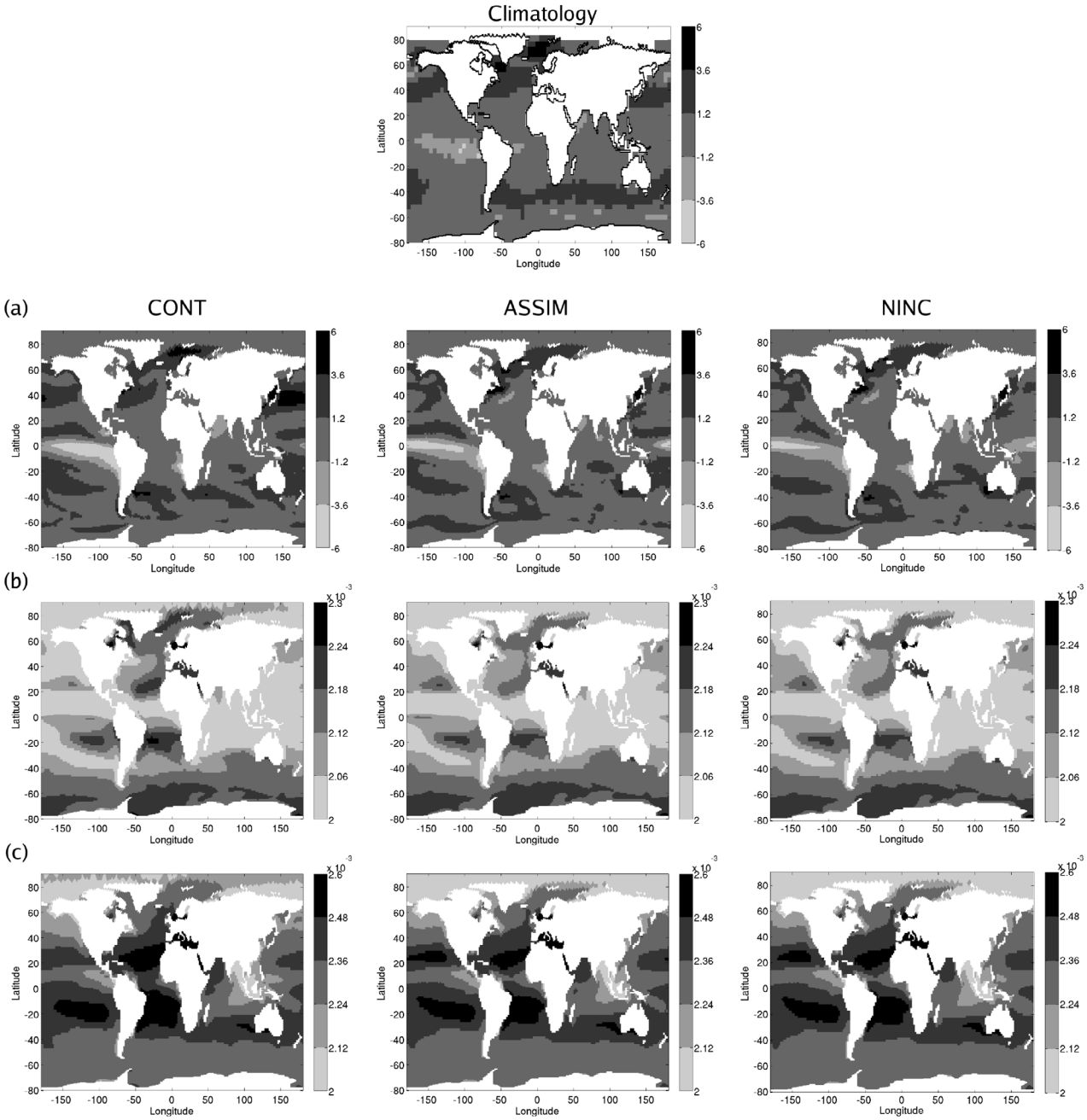

Figure 14. (a) Mean CO_2 flux (in mol/m^2/yr) into the ocean during our analysis period. From left to right the fluxes are for CONT, ASSIM, and NINC. The plot at top shows the Takahashi carbon flux climatology [*Takahashi et al.*, 2009]. Plots show (b) surface DIC (in mol/L) and (c) alkalinity (in eq/L).

processes to also dominate in ASSIM and it is not clear why it has such a small seasonal cycle.

3.3. Iron and Silicate

[23] The mean distributions of the other two nutrients in PlankTOM5, iron and silicate, are shown for CONT and NINC in Figure 7 (results for ASSIM are similar to NINC). The mean iron concentration is not significantly affected by the data assimilation; however, this is not the case for silicate. In both CONT and NINC, silicate is overestimated compared with WOA05, as is seen in Figures 7e and 7f. This is indicative of silicate being less constrained within the model than phosphate. Nonetheless, similar to phosphate, NINC has more surface silicate within the subtropical gyres than CONT, again brought up from depth within the western boundary currents. However, even at the equator there is more silicate in NINC than in CONT, something that did not occur with phosphate. For phosphate the nutrient increment acted to prevent upwelling of additional material, whereas this has been left unconstrained for silicate. This is the likely cause of the excess equatorial silicate. As is shown below, these changes in silicate can have sig-

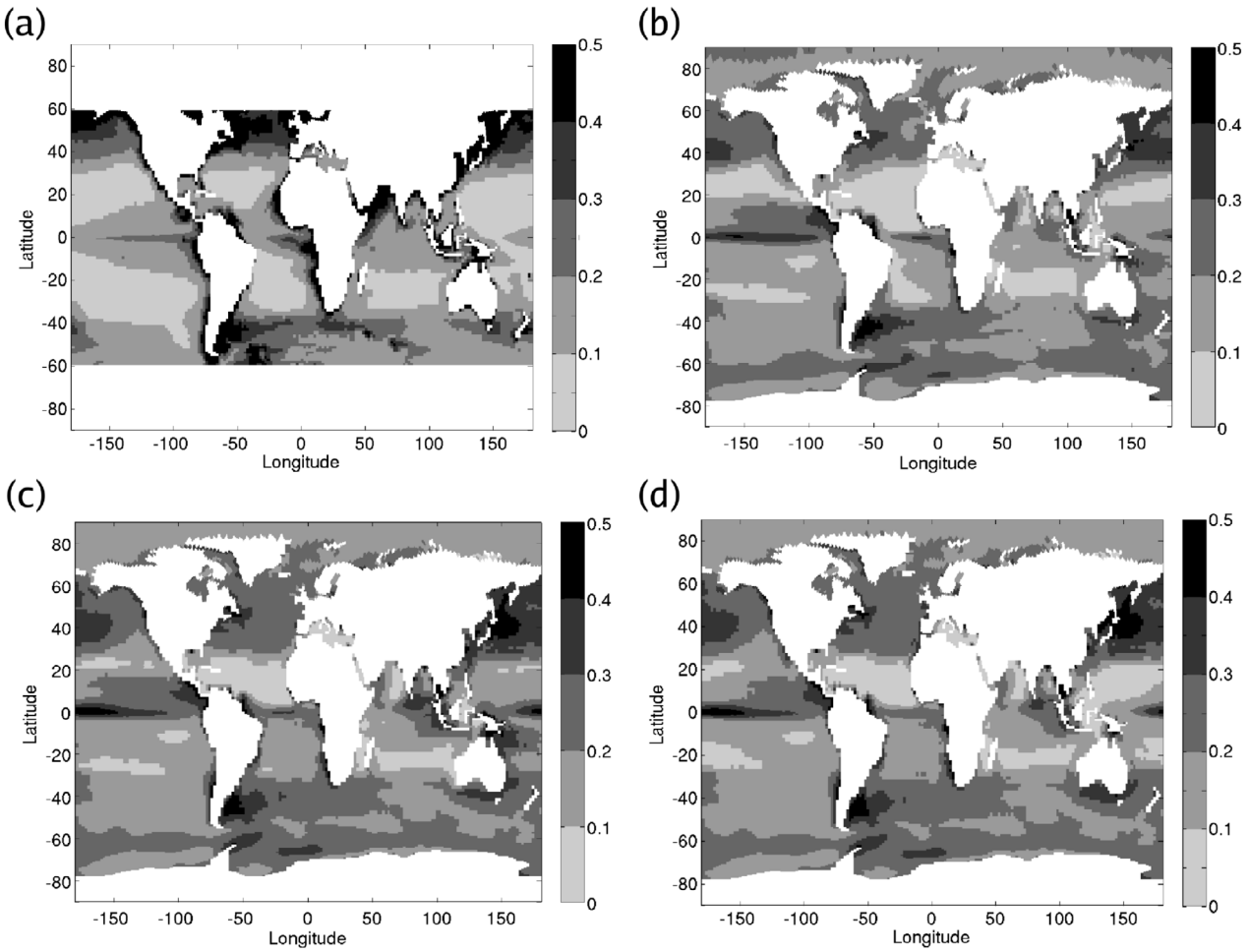

Figure 15. Surface chlorophyll *a* in mg/m^3. (a) Chlorophyll climatology obtained from the SeaWiFS instrument [*O'Reilly et al.*, 2000]. Surface chlorophyll *a* averaged over the analysis period is also given for (b) CONT, (c) ASSIM, and (d) NINC. Note that SeaWiFS chlorophyll for latitudes greater than 60° is masked out because continuous, year-round data are not available at higher latitudes.

nificant impacts on the ecosystem structure particularly the growth of diatoms.

3.4. Carbon Uptake Response

[24] In NINC we have demonstrated an improved representation of temperature, MLD, and, in many areas, phosphate. Here we discuss how this feeds back into the carbon cycle, before discussing the biological response.

[25] Figure 8 shows the globally averaged primary production, export, and air-sea CO_2 flux for CONT, NINC, and ASSIM. Figures 9, 10, and 11 show the same for the equatorial band, and the middle and high latitudes in the Northern Hemisphere, respectively. Additional results for the Southern Hemisphere are given in Figures 12 (midlatitudes) and 13 (high latitudes). Global primary production has systematically increased in NINC and ASSIM. As seen from an examination of the figures, much, and for NINC almost all, of this additional production occurs in midlatitudes, predominantly in the Northern Hemisphere, with the additional production fueled by the increase in nutrients (both phosphate and silicate) in the subtropical gyres. At the equator (Figure 9) NINC initially has ≈1 Pg/yr less production than CONT, though the difference between the two reduces before the end of the analysis period. Conversely, ASSIM shows a moderate increase in production. Again, these changes reflect changes in mean nutrient distribution, although the situation is complex at the equator, with nutrient increases in the Pacific dominating in ASSIM and nutrient decreases in the Atlantic being more important in NINC. At all latitudes the export appears to follow the production, with increased/decreased primary production leading to increased/decreased export. This is especially important at midlatitudes (Figure 10) where increased production-driven export acts to counteract the increase in phosphate in the subtropical gyres. However, it should be noted that for NINC there is one portion of the time series where the primary production and export deviate from proportionality; this is the end of the analysis period in equatorial waters (Figure 9). Here the export continues to be lower in NINC than in CONT, while primary production has become approximately equivalent. This is probably due to horizontal and vertical differences in the production rate, with corresponding differences in the amount of material that is remineralized as it sinks. It should be noted that at high

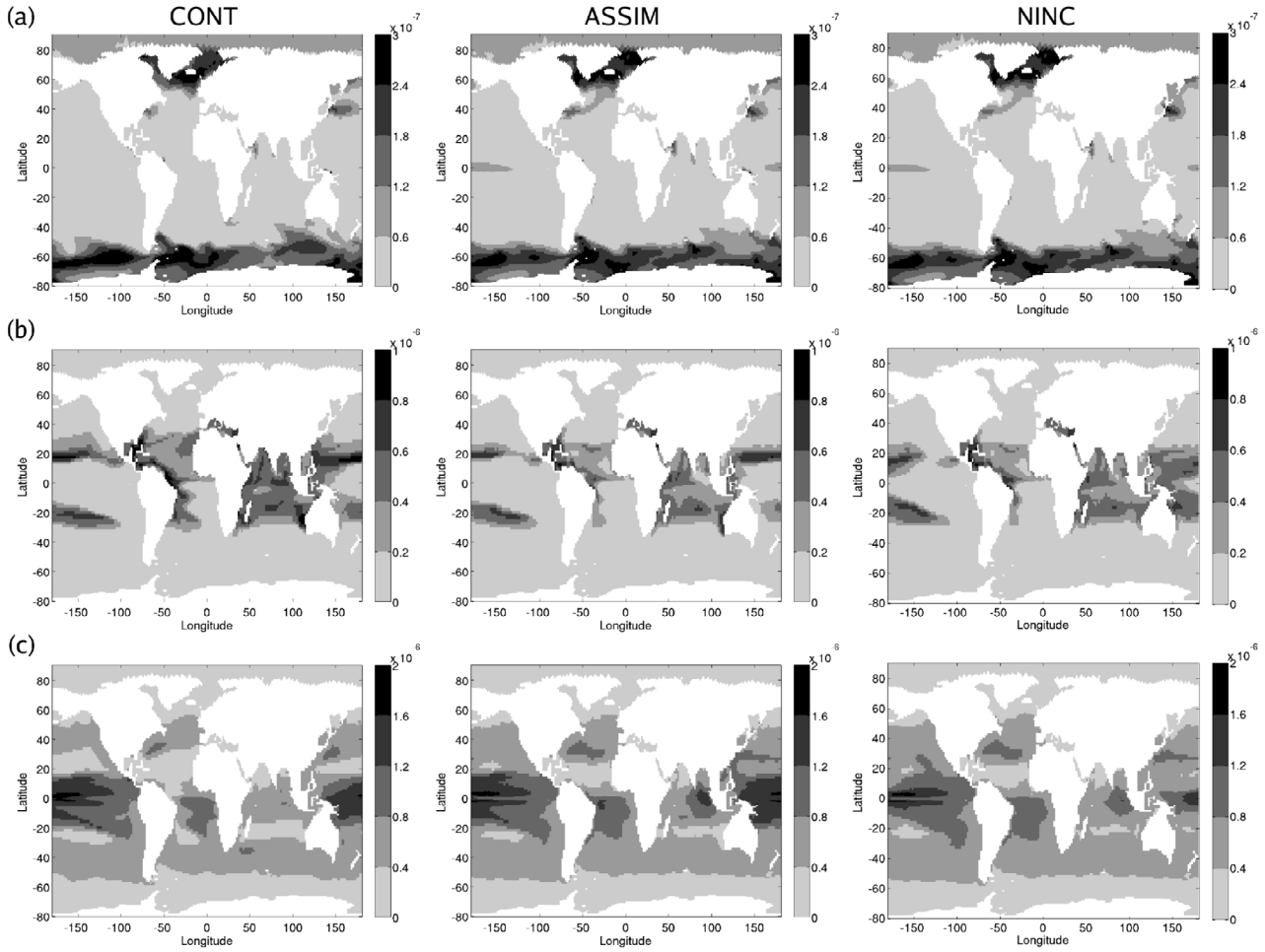

Figure 16. Mean phytoplankton distributions averaged over the analysis period (2000–2007) and down to 313 m depth. Results shown are for (a) diatoms, (b) coccolithophores, and (c) mixed phytoplankton. Left-hand plots are from CONT, middle plots are from ASSIM, and right-hand plots are from NINC. Units are mol/L.

latitudes (Figures 11 and 13), which are less nutrient limited, assimilation and the nutrient increment have had little effect on the primary production or export.

[26] In Figures 8–13 there are significant differences in the air-sea carbon flux between CONT, ASSIM, and NINC. Globally the flux has reduced and become more variable in ASSIM and especially so in NINC. An inspection of the figures shows that changes in flux occur at midlatitudes and near the equator, with fluxes at high latitudes being very similar between the three experiments. At midlatitudes (Figures 10 and 12), NINC and ASSIM have almost identical carbon flux, though their flux is significantly less than in CONT. At the equator (Figure 9), similar to the primary production, ASSIM and NINC show opposite changes (increased and reduced, respectively) air-sea flux. A more detailed look at the air-sea CO_2 flux in Figure 14a shows that the flux reduction in the Northern Hemisphere in NINC and ASSIM is largely due to a reduction in CO_2 flux in the subtropical Pacific, although there is also a reduction in the subtropical Atlantic. This change in flux correlates with increased surface DIC near the Kuroshio, shown in Figure 14b. As with phosphate, we speculate that DIC is being advectively brought to the surface within the boundary current. The influence of alkalinity in this region (Figure 14c) looks to be small, as there is relatively little difference between CONT and the other runs. However, alkalinity may have more influence at similar latitudes in the Atlantic, with both NINC and ASSIM showing reduced levels. Within a few degrees of the equator in the western Pacific, both ASSIM and NINC outgas more than CONT; however, immediately north and south of this region significant ingassing is observed in ASSIM, but not NINC. It is these patterns of equatorial CO_2 flux that cause the reduction in mean flux in NINC and the concomitant increase in ASSIM that is seen in Figure 9. The cause of the increased flux seen in ASSIM is not clear, but is probably due to additional primary production (see Figure 9) exporting carbon down from the surface. In the Southern Hemisphere, changes in flux are smaller than in the Northern Hemisphere, as are changes to DIC and alkalinity. However, small changes are present with

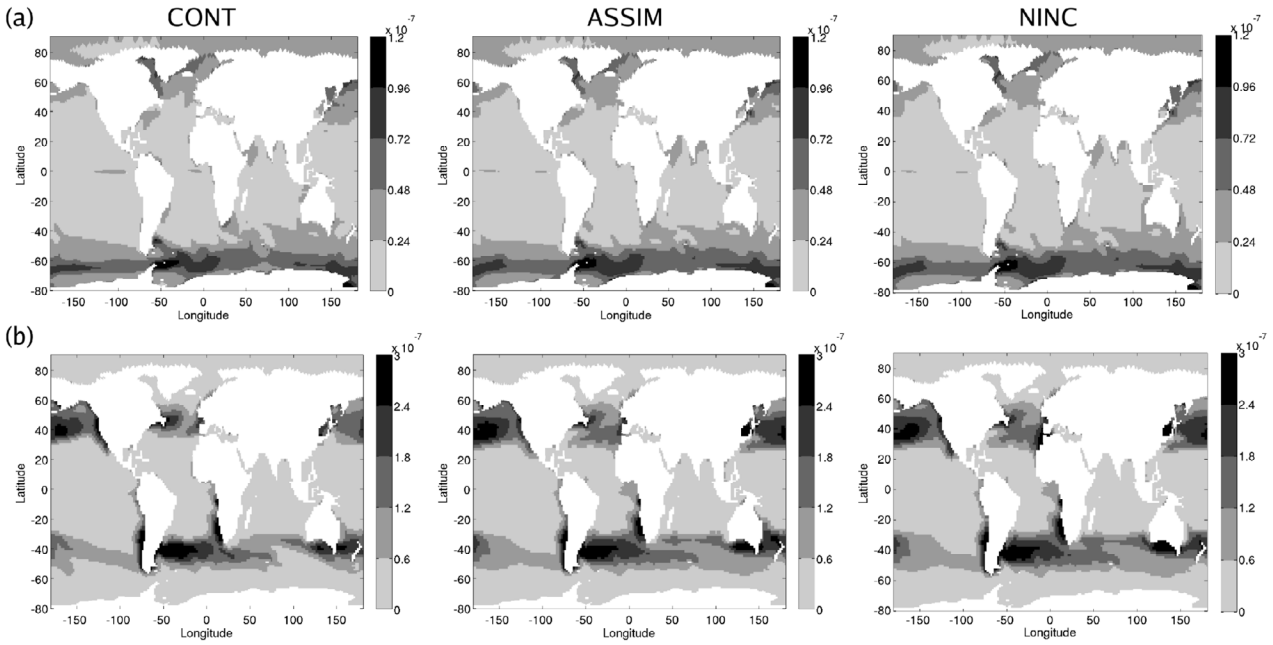

Figure 17. Mean zooplankton distributions averaged over the analysis period (2000–2007) and down to 313 m depth. Results shown are for (a) microzooplankton and (b) mesozooplankton. Left-hand plots are from CONT, middle plots are from ASSIM, and right-hand plots are from NINC. Units are mol/L.

significant differences apparent in the Indian Ocean and both NINC and ASSIM having increased carbon flux near 60°S in the Pacific.

3.5. Biological Response

[27] Turning to the biology itself, Figure 15 shows the mean surface chlorophyll distribution of CONT, ASSIM, and NINC alongside a climatology obtained from the SeaWiFS satellite instrument [*O'Reilly et al.*, 2000]. Discounting coastal waters, for which SeaWiFS chlorophyll is known to be poor [*Hu et al.*, 2000], an inspection reveals that assimilation has significantly increased chlorophyll in the subtropical gyres and Kuroshio compared with either CONT or SeaWiFS. This is what we expect given the results discussed above, with increased primary production driven by more nutrient upwelling leading to the additional chlorophyll. At high latitudes (above 40°N), NINC and ASSIM have chlorophyll distributions that are broadly similar and that tend to be slightly higher than CONT, especially in the Atlantic. In this region, nutrient concentrations are high (see Figures 2 and 4) and grazing is likely to be a stronger control on the biology than phosphate. However, near the equator in the western Pacific substantive differences are present. In particular, ASSIM displays too much chlorophyll relative to SeaWiFS between 20°S and 20°N. CONT, while superior to ASSIM, also displays this bias. However, NINC, which has relatively low equatorial phosphate, is a much closer match to SeaWiFS.

[28] The ecosystem structure underlying the chlorophyll patterns is shown in Figure 16 (phytoplankton) and Figure 17 (zooplankton). It can quickly be seen that within the subtropical gyres the elevated chlorophyll in NINC and ASSIM is due to an abundance of mixed phytoplankton, whose growth has been driven by increased nutrient availability. Interestingly, in these two runs coccolithophores show reduced concentration in the subtropical gyres. This is probably due to increased predation by zooplankton, and a careful inspection of Figure 17 does show increases in zooplankton concentrations in the northern regions of the subtropical gyres. Diatoms, which are more nutrient limited than mixed phytoplankton, show negligible change within the subtropical gyres between the three models.

[29] Away from the subtropical gyres, diatoms increase in the equatorial Pacific in NINC and ASSIM, while mixed phytoplankton decrease. This is again a response to changes in nutrient distribution, but here a systematic increase in silicate (see Figure 7) is the cause. Diatoms also increase along the Gulf Stream in ASSIM and NINC, but it is less clear that this increase is due to changes in the silicate distribution. When compared to CONT, mixed phytoplankton in NINC are reduced in equatorial latitudes, particularly the western Pacific, which leads to the improvement in chlorophyll noted above, and this change can be linked to the improvement in phosphate seen in Figure 2. Conversely ASSIM, which shows increased phosphate bias at the equator, shows an increase in mixed phytoplankton (and thus chlorophyll) relative to CONT. As with the subtropical gyres, changes to the coccolithophore population are likely to be due to changes in zooplankton predation; however, due to the relative differences in zooplankton concentrations between high and low latitudes, these changes are not visible in Figure 17.

4. Discussion

[30] The assimilation of physical data into global physical-biogeochemical models is a vital step in performing biogeo-

chemical modeling with realistic mixed layer depths and temperatures. A key step is to demonstrate that the nutrient distributions in such experiments are improved as nutrients, along with the physical ocean state, exert a direct control on the biology.

[31] The key innovation of this paper is to introduce a nutrient increment to the physical data assimilation process, a technique of low computational cost that maintains the nutrient-density relationship within each water column through an assimilation cycle. The aim is to reduce the transfer of nutrients between water masses which can lead to bias. An experiment was conducted to test the nutrient increment, whereby phosphate was incremented within a 17 year run of the NEMO 2° modeling framework. When compared against a control run with no assimilation, phosphate bias against climatological values was reduced both near the equator and at high latitudes. However, the real significance of the method became apparent when it was compared against a run which assimilated temperature and salinity data, but did not include a correction to the nutrient field. In this case, assimilation upset the balance between nutrients and the physical state of the model and caused significant nutrient biases. Away from the subtropical gyres, these biases were much reduced by the nutrient increment, demonstrating that the method was capable of correcting for this type of error. Thus, to avoid such biases in the future, a nutrient incrementing scheme should always be considered when assimilating physical data into an ocean-biogeochemical model.

[32] In addition to changes in the nutrient structure, the effects of the nutrient increment have been shown to feed through into both the bulk biological properties of the ocean and into changes in ecosystem plankton dynamics. Of note are the chlorophyll improvements, when compared against SeaWiFS, and changes to air-sea carbon flux observed in the equatorial west Pacific.

[33] In all, our results indicate a way forward for further improving nutrient distributions in models of the world's oceans, although some key problems remain. Principally the advective upwelling of nutrients into the subtropical gyres is a dominant issue. This problem may be alleviated at higher model resolutions where the boundary currents would be better resolved.

[34] It may also be possible to extend the nutrient increment methodology to other nutrients, such as silicate and iron; however, this will require the use of higher-vertical-resolution models that can resolve nutrient-density relationships in the presence of large vertical gradients. Ultimately this work could be incorporated into an assimilation scheme that directly assimilates nutrient data. Such a scheme could be conceptually similar to the salinity-temperature scheme of *Haines et al.* [2006] and *Smith and Haines* [2009] where the observational nutrient increment would become an extra term in the assimilation equations.

[35] **Acknowledgments.** The authors thank Erik Bruintenhuis of the University of East Anglia for his help in the setting up and running of the PlankTOM5 model. We would thank the DRAKKAR consortium for providing us with the forcing fields used in our model runs. This work was funded as part of the MarQUEST program, a subset of the QUEST program, and was funded by Natural Environment Research council grant NE/C516095/1.

References

Anderson, L., A. Robinson, and C. Lozano (2000), Physical and biological modeling in the Gulf Stream region: I. Data assimilation methodology, *Deep Sea Res., Part I*, *47*, 1787–1827.

Antonov, J. I., R. A. Locarnini, T. P. Boyer, A. Mishonov, and H. E. Garcia (2006), Salinity, in *World Ocean Atlas 2005*, vol. 2, edited by S. Levitus, U.S. Gov. Print. Off., Washington, D. C. (Available at http://www.nodc.noaa.gov/OC5/WOA05/)

Aumont, O., E. Maier-Reimer, S. Blain, and P. Monfray (2003), An ecosystem model of the global ocean including Fe, Si, P colimitations, *Global Biogeochem. Cycles*, *17*(2), 1060, doi:10.1029/2001GB001745.

Beardall, J., E. Young, and S. Roberts (2001), Approaches for determining phytoplankton nutrient limitation, *Aquat. Sci.*, *63*, 44–69.

Bloom, S. C., L. L. Takacs, A. M. da Silva, and D. Ledvina (1996), Data assimilation using incremental analysis updates, *Mon. Weather Rev.*, *124*, 1256–1271.

Brodeau, L., B. Barnier, A. Treguir, T. Penduff, and S. Gulev (2009), An ERA40-based atmospheric forcing for global ocean circulation models, *Ocean Modell.*, *31*, 88–104.

Buitenhuis, E., et al. (2006), Biogeochemical fluxes through mesozooplankton, *Global Biogeochem. Cycles*, *20*, GB2003, doi:10.1029/2005GB002511.

Carmillet, V., J. Brankart, P. Brasseur, H. Drange, G. Evensen, and J. Verron (2001), A singular evolutive extended Kalman filter to assimilate ocean color data in a coupled physical-biochemical model of the North Atlantic Ocean, *Ocean Modell.*, *3*, 167–192.

de Boyer Montégut, C., G. Madec, A. Fischer, A. Lazar, and D. Iudicone (2004), Mixed layer depth over the global ocean: An examination of profile data and a profile-based climatology, *J. Geophys. Res.*, *109*, C12003, doi:10.1029/2004JC002378.

Eden, C., and A. Oschlies (2006), Adiabatic reduction of circulation-related CO_2 air-sea flux biases in a North Atlantic carbon cycle model, *Global Biogeochem. Cycles*, *20*, GB2008, doi:10.1029/2005GB002521.

Fichefet, T., and M. Morales Maqueda (1997), Sensitivity of a global sea ice model to the treatment of ice thermodynamics and dynamics, *J. Geophys. Res.*, *102*(C6), 12,609–12,646.

Fichefet, T., and M. Morales Maqueda (1999), Modelling the influence of snow accumulation and snow-ice formation on the seasonal cycle of the Antarctic sea-ice cover, *Clim. Dyn.*, *15*, 251–268.

Fox, A., and K. Haines (2003), Interpretation of water mass transformations diagnosed from data assimilation, *J. Phys. Oceanogr.*, *33*, 485–498.

Garcia, H. E., R. A. Locarnini, T. P. Boyer, and J. I. Antonov (2006), Nutrients, in *World Ocean Atlas 2005*, vol. 4, edited by S. Levitus, U.S. Gov. Print. Off., Washington, D. C. (Available at http://www.nodc.noaa.gov/OC5/WOA05/)

Gent, R. P., and J. C. McWilliams (1990), Isopycnal mixing in ocean circulation models, *J. Phys. Oceanogr.*, *20*, 150–155.

Gregg, W. (2007), Assimilation of SeaWiFS ocean chlorophyll data into a three-dimensional global ocean model, *J. Mar. Syst.*, *69*(3-4), 205–225, doi:10.1016/j.jmarsys.2006.02.015.

Haines, K., J. D. Blower, J.-P. Drecourt, C. Liu, A. Vidard, I. Astin, and X. Zhou (2006), Salinity assimilation using S(T): Covariance relationships, *Mon. Weather Rev.*, *134*, 759–771.

Hemmings, J., R. Barciela, and M. Bell (2008), Ocean color data assimilation with material conservation for improving model estimates of air-sea CO_2 flux, *J. Mar. Res.*, *66*, 87–126.

Hu, C., K. Carder, and F. Muller-Karger (2000), Atmospheric correction of SeaWiFS imagery over turbid coastal waters: A practical method, *Remote Sens. Environ.*, *74*, 195–206.

Ingleby, B., and M. Huddleston (2007), Quality control of ocean temperature and salinity profiles—Historical and real-time data, *J. Mar. Syst.*, *65*, 158–175.

Large, W., and S. Yeager (2004), Diurnal to decadal global forcing for ocean and sea ice-ice models: The data sets and flux climatologies, *NCAR Tech. Note, NCAR/TN-460+STR*, Natl. Cent. for Atmos. Res., Boulder, Colo.

Le Quéré, C., et al. (2005), Ecosystem dynamics based on plankton functional types for global ocean biogeochemistry models, *Global Change Biol.*, *11*, 2016–2040.

Locarnini, R. A., A. Mishonov, J. I. Antonov, T. P. Boyer, and H. E. Garcia (2006), Temperature, in *World Ocean Atlas 2005*, vol. 1, edited by S. Levitus, U.S. Gov. Print. Off., Washington, D. C. (Available at http://www.nodc.noaa.gov/OC5/WOA05/)

Losa, S. N., G. A. Kivman, J. Schröter, and M. Wenzel (2003), Sequential weak constraint parameter estimation in an ecosystem model, *J. Mar. Syst.*, *43*(1-2), 31–49.

Madec, G. (2008), NEMO reference manual, ocean dynamics component, Inst. Pierre-Simon Laplace, Paris. (Available at http://www.nemo-ocean.eu/)

Martin, M., A. Hines, and M. Bell (2007), Data assimilation in the FOAM operational short-range ocean forecasting system: A description of the scheme and its impact, *Q. J. R. Meteorol. Soc.*, *133*, 981–995.

Ming, J., and A. Leetmaa (1997), Impact of data assimilation on ocean initialization and El Niño prediction, *Mon. Weather Rev.*, *125*, 742–753.

Natvik, L.-J., and G. Evensen (2002), Assimilation of ocean colour data into a biochemical model of the North Atlantic: part 1. Data assimilation experiments, *J. Mar. Syst.*, *40-41*, 127–153.

Nerger, L., and W. Gregg (2007), Assimilation of SeaWiFS data into a global ocean-biogeochemical model using a local SEIK filter, *J. Mar. Syst.*, *68*, 237–254.

O'Reilly, J., et al. (2000), SeaWiFS postlaunch calibration and validation analyses: Part 3, *NASA Tech. Memo, 2000-206892*, vol. 11, 49 pp., edited by S. B. Hooker and E. R. Firestone, NASA Goddard Space Flight Cent., Greenbelt, Md. (Available at http://oceancolor.gsfc.nasa.gov/cgi/postlaunch_tech_memo.pl)

Ridgwell, A., J. Hargreaves, N. Edwards, J. Annan, T. Lenton, R. Marsh, A. Yool, and A. Watso (2007), Marine geochemical data assimilation in an efficient Earth system model of global biogeochemical cycling, *Biogeosciences*, *4*, 87–104.

Smith, G., and K. Haines (2009), Evaluation of the S(T) assimilation method with the Argo database, *Q. J. R. Meteorol. Soc*, *135*, 739–756.

Smolarkiewicz, P. K. (1983), A simple positive definite advection scheme with small implicit diffusion, *Mon. Weather Rev.*, *111*, 479–486.

Sweeny, C., E. Gloor, A. R. Jacobson, R. M. Key, G. McKinley, J. L. Sarmiento, and R. Wanninkhof (2007), Constraining global air-sea gas exchange for CO_2 with recent ^{14}C measurements, *Global Biogeochem. Cycles*, *21*, GB2015, doi:10.1029/2006GB002784.

Takahashi, T., et al. (2009), Climatological mean and decadal changes in surface ocean pCO_2, and net sea-air CO_2 flux over the global oceans., *Deep Sea Res., Part II*, *56*, 554–577.

Troccoli, A., and K. Haines (1999), Use of the temperature-salinity relation in a data assimilation context, *J. Atmos. Oceanic Technol.*, *16*, 2011–2025.

Uppala, S., et al. (2005), The ERA-40 reanalysis, *Q. J. R. Meteorol. Soc.*, *131*, 2961–3012.

Wanninkhof, R. (1992), Relationship between wind-speed and gas exchange over the ocean, *J. Geophys. Res.*, *97*, 7373–7382.

While, J., and K. Haines (2010), A comparison of the variability of biological nutrients against depth and potential density, *Biogeosciences*, *7*, 1263–1269.

Zalesak, S. (1979), Fully multidimensional flux-corrected transport algorithms for fluids, *J. Comp. Phys.*, *31*, 335–362.

Zhao, L., H. Wei, Y. Xu, and S. Feng (2005), An adjoint data assimilation approach for estimating parameters in a three dimensional ecosystem model, *Ecol. Modell.*, *186*(2), 234–249.

K. Haines, Environmental Systems Science Centre, University of Reading, Harry Pitt Building, 3 Earley Gate, Reading RG6 6AL, UK.

G. Smith, Management Research Division/Atmospheric Science and Technology Directorate, Environment Canada, Dorval, Quebec H9P 1J3, Canada.

J. While, UK Met Office, Fitzroy Rd., Exeter EX1 3PB, UK. (james.while@metoffice.gov.uk)